

Lyman α emitting galaxies at $0.2 < z < 0.35$ from GALEX spectroscopy

Jean-Michel Deharveng¹, Todd Small², Tom A. Barlow², Céline Péroux¹, Bruno Milliard¹, Peter G. Friedman², D. Christopher Martin², Patrick Morrissey², David Schiminovich³, Karl Forster², Mark Seibert², Ted K. Wyder², Luciana Bianchi⁴, Jose Donas¹, Timothy M. Heckman⁵, Young-Wook Lee⁶, Barry F. Madore⁷, Susan G. Neff⁸, R. Michael Rich⁹, Alex S. Szalay⁵, Barry Y. Welsh¹⁰, Sukyoung K. Yi⁶,

ABSTRACT

The *GALEX* (*Galaxy Evolution Explorer*) spectroscopic survey mode, with a resolution of $\sim 8 \text{ \AA}$ in the FUV (1350 - 1750 \AA) and $\sim 20 \text{ \AA}$ in the NUV (1950 - 2750 \AA) is used for a systematic search of Ly α emitting galaxies at low redshift. This aims at filling a gap between high-redshift surveys and a small set of objects studied in detail in the nearby universe. A blind search of 7018 spectra extracted in 5 deep exposures (5.65 sq.deg) has resulted in 96 Ly α emitting galaxy candidates in the FUV domain, after accounting for broad-line AGNs. The Ly α EWs (equivalent width) are consistent with stellar population model predictions and show no trends as a function of UV color or UV luminosity, except a possible decrease in the most luminous that may be due to small-number statistics. Their

¹Laboratoire d'Astrophysique de Marseille, BP 8, Traverse du Siphon, 13376 Marseille Cedex 12, France

²California Institute of Technology, MC 405-47, 1200 East California Boulevard, Pasadena, CA 91125

³Department of Astronomy, Columbia University, New York, NY 10027

⁴Center for Astrophysical Sciences, The Johns Hopkins University, 3400 N. Charles St., Baltimore, MD 21218

⁵Department of Physics and Astronomy, The Johns Hopkins University, Homewood Campus, Baltimore, MD 21218

⁶Center for Space Astrophysics, Yonsei University, Seoul 120-749, Korea

⁷Observatories of the Carnegie Institution of Washington, 813 Santa Barbara St., Pasadena, CA 91101

⁸Laboratory for Astronomy and Solar Physics, NASA Goddard Space Flight Center, Greenbelt, MD 20771

⁹Department of Physics and Astronomy, University of California, Los Angeles, CA 90095

¹⁰Space Sciences Laboratory, University of California at Berkeley, 601 Campbell Hall, Berkeley, CA 94720

distribution in EW is similar to that at $z \sim 3$ but their fraction among star-forming galaxies is smaller. Avoiding uncertain candidates, a sub-sample of 66 objects in the range $0.2 < z < 0.35$ has been used to build a Ly α LF (luminosity function). The incompleteness due to objects with significant Ly α emission but a UV continuum too low for spectral extraction has been evaluated. A comparison with H α LF in the same redshift domain is consistent with an average Ly α /H α of ~ 1 in about 15 % of the star-forming galaxies. A comparison with high-redshift Ly α LFs implies an increase of the Ly α luminosity density by a factor of about 16 from $z \sim 0.3$ to $z \sim 3$. By comparison with the factor 5 increase of the UV luminosity density in the same redshift range, this suggests an increase of the average Ly α escape fraction with redshift.

Subject headings: galaxies: evolution — galaxies: luminosity function — galaxies: ISM — galaxies: starburst — ultraviolet: galaxies

1. Introduction

The Lyman α emission line has attracted large attention as a spectral signature for identifying galaxies and securing redshifts at large distances. This emission line, however, is fraught with difficulty. Because Ly α photons are resonantly scattered by neutral hydrogen, they may suffer more dust attenuation than adjacent UV continuum photons; their escape is also affected by the relative geometries of neutral and ionized interstellar gas, and, last but not least, by the velocity structure of neutral gas. The first two factors have been extensively discussed in the light of IUE observations of nearby star-forming galaxies (Giavalisco, Koratkar, & Calzetti 1996) (and references therein) and with model calculations (Charlot & Fall 1993; Neufeld 1991; Chen & Neufeld 1994) (and references therein). The crucial role of the velocity structure of neutral gas has been shown by the HST spectra of nearby star-forming galaxies (Kunth et al. 1998; Mas-Hesse et al. 2003). Similar evidence was offered by the spectra of Lyman Break Galaxies (LBG) (Pettini et al. 1998, 2000). Ly α photons mainly escape when they are scattered off neutral gas that is offset in velocity from the bulk of the ionized regions. The complexity of the escape of Ly α emission is also well illustrated by the broad distribution of Ly α strengths and profile-types observed in the LBG spectroscopic sample of Shapley et al. (2003). The Ly α transmission mechanisms, especially the resulting emergent line profiles, have since been investigated in increasingly realistic models (e.g.) (Ahn, Lee, & Lee 2001, 2002, 2003; Hansen & Oh 2006; Verhamme, Schaerer & Maselli 2006). An extensive review of all the aspects of the observations of the Ly α emission line in galaxies has been recently given by Schaerer (2007).

The complex nature of Ly α escape was advocated for the disappointing results of earlier searches of distant Ly α emitters (e.g.) (Djorgovski & Thompson 1992). Nonetheless, the Ly α emission remains the only mean for identifying galaxies when the continuum becomes too faint to be detected, and, following Cowie & Hu (1998) and Hu, Cowie, & McMahon (1998), increasingly deeper and larger surveys have come into a widespread use for detecting galaxies at high redshifts. Beyond the redshift of ~ 6 , the increasingly neutral IGM is not a complete obstacle to the visibility of Ly α emission (e.g.) (Haiman 2002) and the density evolution of Ly α emitters may even help to trace the history of the cosmic re-ionization (e.g.) (Malhotra & Rhoads 2004; Stern et al. 2005; Kashikawa et al. 2006).

Although nearby galaxies have played a key role for understanding the factors affecting Ly α escape, their observations, using space-borne UV spectrographs in pointing mode, were directed to specific and known objects. As a consequence, there is not yet a systematic survey for redshifts smaller than those reachable from the ground. We use here the *GALEX* spectroscopic survey mode for the first systematic search of Ly α emitting galaxies at low redshift. Goals are to understand (i) whether the Ly α escape is related to specific properties of galaxies, (ii) whether the Ly α emission evolves from current epoch to high z as the cosmic star formation rate traced by Balmer lines or the UV continuum of galaxies. If so, the average relationship between the massive stellar content of the galaxies and the Ly α emission would be constant over time; the Ly α emission might be used as a tracer of star formation, with an empirical calibration encapsulating the average effects of resonant scattering. If not, there would be an evidence for cosmic evolution of the physical processes, especially galactic winds, expected to play a central role in the Ly α escape from galaxies.

2. Data analysis

2.1. *GALEX* ultraviolet spectroscopy and selection of line emitters

The *GALEX* instrument and mission are described by Martin et al. (2005) and Morrissey et al. (2005). The spectroscopy mode utilizes a CaF₂ grism that can be moved into the convergent beam of the telescope to form simultaneous spectra of all sources in the field in both FUV and NUV bands. The usable wavelength range for relatively faint sources is approximately 1350 to 1750 Å for FUV (2nd order) and 1950 to 2750 Å for NUV (1st order). The spectral resolution for a point source (assuming a 5 arcsecond PSF) is ~ 8 Å for FUV and ~ 20 Å for NUV. Details on the observations (multiple grism orientations in order to avoid the spectra overlap) and the various steps of data reduction are given by Morrissey et al. (2007). The spectral extraction is performed for all point sources in the direct image observations exceeding a S/N limit per resolution element in the co-added results of 2 in FUV and 3 in

NUV. Each resulting spectrum is a one-line image of 488 pixels with 3.5 \AA per pixel and starting at 1300 \AA .

Eleven fields observed in spectroscopy mode are available from the *GALEX* GR2. In order to keep a relative homogeneity in the detection depth and related selection effects we have concentrated on five fields with an exposure time larger than 70,000 s and covering an area of 5.65 square deg. The characteristics of these five fields are summarized in Table 1, with the total number of spectra extracted by the reduction pipeline and the number of objects identified in the same fields with the direct imaging mode. Each spectrum has been visually inspected and potential Ly α emission features have been measured (central wavelength, line flux, equivalent width and full width at half maximum, FWHM) with the IRAF splot package (gaussian fitting). The signal to noise ratio does not permit reasonable identifications of Ly α absorption.

The objects with a FWHM larger than about 15 \AA in the FUV domain and about 27 \AA in the NUV are classified as broad-line AGNs. These limits are based on the minimum value of 1200 km s^{-1} , observed in the distribution of the FWHM of H α emission line of galaxies in the SDSS (Hao et al. 2005a) and found to make a separation between the broad-line AGNs and other emission-line objects. These limits take into account the average redshift and the spectral resolution in the respective GALEX UV bands. The presence/absence of emission lines such as OVI, CIII, CIV, when the redshift is appropriate and the brightness large enough for detection in the GALEX bands, is also used to confirm the classification, especially when the FWHM values are close to the limit values.

In the NUV domain, only broad-line AGNs are found according to our criterions. This is consistent with the NUV (AB) limiting magnitude of 22 of the vast majority of extracted spectra. At the redshift of 0.65, the lowest redshift at which a Ly α emitter can be detected in the NUV band, this flux limit would imply an (AB) absolute magnitude brighter than -21 , a value extreme and rare for galaxies, as shown by the evolution of the galaxy 1500 \AA luminosity function (Arnouts et al. 2005). This situation is aggravated by the dilution of narrow spectral features into the $\sim 20 \text{ \AA}$ NUV spectral resolution which plays against the detection of Ly α emitting galaxies.

It is found impossible to identify narrow-line AGNs among our potential Ly α emitting galaxies because either their associated CIV line is redshifted into the noisy wavelength domain between the FUV and NUV, or the object is too faint for a detection of the CIII or CIV lines. A contamination by narrow-line AGNs is probably present and it will be seen in the next subsection whether additional spectral information can help.

As our blind search was open to all extracted spectra and not limited to galaxies with

the appropriate redshift, we have an increased risk of spurious detections. We have therefore classified our candidates into three categories (good, fair and uncertain) in order to try to control if the properties of our objects depend on the quality of their identification, even though the sample sizes are changing. Fig. 1 gives a few examples of these spectra with the proposed identification. The identification of potential Ly α features is also hampered at both ends of the spectral range by fluctuations that increase because of the decrease in efficiency. In between, the useful spectral range is not constant from object to object. For the problems that require a control of the volume surveyed, we have defined the largest wavelength domain that we have been able to search in relatively uniform conditions for all the objects. This wavelength range 1459 – 1642 Å translates in a redshift window 0.2 – 0.35 for the Ly α emission line.

The number of Ly α emission line candidates resulting from our blind search, as well as those retained for the discussion of luminosity functions (quality 1 and 2 only; $0.2 < z < 0.35$) are listed in Table 1 for each field investigated. The total numbers are 96 and 66 respectively in these two categories. Table 2 summarizes the main characteristics of our candidates with the line flux of the emission features, and, assuming an identification to Ly α emission, the redshift and the derived Ly α luminosity. The line fluxes and Ly α luminosities include a correction factor resulting from a re-calibration of the spectral response, that was verified to make no systematic differences on average between the direct image photometry and the fluxes derived from an integration of the spectra. The one-sigma precision on the line flux measurement is of the order of 4×10^{-16} erg cm $^{-2}$ s $^{-1}$. In combination with an evaluation of the uncertainty in the determination of the UV continuum adjacent to the emission line, this number gives a precision on the equivalent width (EW) from about 25 % at EW \sim 20 Å to 15 % at EW \sim 100 Å.

2.2. Cross-verification with spectroscopic or photometric redshift information

As a control of our blind search, we have compared our results with existing information about each candidate, especially any redshift from spectroscopy or photometry in the optical. We are mostly concerned by spurious features and not confusion with another emission line since Ly α emission is known as unique in the FUV spectra of galaxies. The possibility of identifying narrow-line AGNs would also be of interest since we have shown it was difficult in practice with the UV spectra alone.

Each of our 96 candidates was searched in the NED (NASA/IPAC Extragalactic Database) and the recent Data Release 3 of DEEP2 (Davis et al. 2007); the 14 redshifts found are displayed in Table 2. Only one of these redshifts, based on COMBO-17 photometric measure-

ments (Wolf et al. 2004) and possibly affected by misidentification in a dense group, is in significant disagreement with the evaluation based on the Ly α emission. All 14 objects are classified as galaxies. Although this cross-verification is presently limited to a small subset of candidates, it is seen as an encouraging validation of our approach. The small number of redshifts available from the visible was somewhat expected: on one hand, the SDSS spectroscopic survey (available in 3 of our 5 fields) has a small fraction of galaxies at $z > 0.2$, on the other hand the *GALEX* spectroscopy is not deep enough for overlapping well the specific and deep redshift surveys with large telescopes.

3. Properties of the Ly α emitting galaxies

3.1. Comparison with the UV-selected galaxy population

Our Ly α emitting galaxy candidates are compared with the other UV sources of *GALEX*, especially those identified as galaxies, in order to see whether the presence of the Ly α line is related to any galaxy property. Such a comparison can also illustrate the importance of selection effects. In the plot of the FUV flux vs. UV color, the 96 Ly α emitting candidates lie at the faint magnitude and blue color boundaries of the domain occupied by the 736 objects classified as galaxies but without Ly α features. The faint magnitude boundary has a natural explanation with our candidates being faint since in principle at $z > 0.2$. The blue color boundary has two possible explanations. On one hand, easier Ly α escape may come with less dust and bluer color; on the other hand, bluer color may imply a higher FUV continuum flux and easier detection of emitting features.

Another aspect of the comparison of our Ly α emitting candidates with respect to the general population of *GALEX* sources is shown in Fig. 2 with the distribution of the FUV magnitudes. This distribution is displayed for four samples, the UV sources detected in the images, the extracted spectra, the objects classified as galaxies (without any emission feature) and the Ly α emitting galaxy candidates. The spectra appear to have been systematically extracted down to a magnitude of 21.5, a level at which samples are complete according to the completeness analysis of *GALEX* images by Xu et al. (2005). The distribution of objects classified as galaxies also peak at this limit. At the bright end of the distribution, the proportion of galaxies with Ly α emission is naturally low since the objects are selected at $z > 0.2$. At the faint end, the number of objects classified as galaxies and the number of Ly α emitting galaxy candidates are very similar. This does not mean that all identified faint galaxies have Ly α in emission since the samples are by construction distinct. This tells that the identification of faint galaxies is relatively easier with than without an emission feature. The distribution of Ly α emitting galaxy candidates peak at 21.5 – 22 magnitude. They are

clearly affected by incompleteness.

3.2. Distribution of Ly α EW

The distribution of Ly α rest-frame equivalent widths is displayed in Fig. 3. Beyond a completeness limit at about 20 Å, the distribution is comparable with that of Shapley et al. (2003) for LBGs at $z \sim 3$. The fraction of Ly α emitting galaxies (with EW > 20 Å) relative to the number of star-forming galaxies in the redshift range $0.2 < z < 0.35$ cannot be determined directly because redshift measurements are available only in limited areas and, in these areas, the number of matches with *GALEX* spectra is very small. We can rely on evaluations based on the *GALEX* far-UV survey and use the luminosity functions derived by Arnouts et al. (2005) in the redshift range $0.2 < z < 0.4$ to calculate the total number of galaxies up to a given magnitude in a volume comparable to our observed volume. Up to magnitude (AB) of 21 and 21.5, the number of Ly α emitting galaxies with EW > 20 Å are respectively 9 (out of 58) and 36 (out of 243), corresponding to a fraction of 15 % of the total number of (star-forming) galaxies. This fraction is lower than the fraction of 25 % reported by Shapley et al. (2003) for LBGs at $z \sim 3$. This difference may reflect differences between the methods of evaluation. The spectroscopic sample of Shapley et al. (2003) does not have a UV flux limit as we had to use for the determination of the size of the parent population since our candidates are searched among objects of unknown redshifts. On the other hand, the difference is consistent with the trend of lower incidence of Ly α emission at low redshift found by Reddy et al. (2007); they, however, report a fast decline of the fraction of Ly α emitting galaxies (EW > 20 Å) with a value of 8 % in the redshift bin $1.9 < z < 2.17$.

The Ly α rest-frame EWs displayed in Fig. 3 are consistent with the large spread of values predicted by the stellar population models of Charlot & Fall (1993) and any amount of Ly α quenching in the resonant scattering process. The EW values larger than model predictions that raise problems at high redshift (Shimasaku et al. 2006; Finkelstein et al. 2007; Stanway et al. 2007) are not found.

3.3. Ly α dependences: *GALEX* data

We also examine how the Ly α strength varies across our sample as a function of different galaxy parameters. The most obvious parameters are those relative to the UV continuum emission as obtained from *GALEX* photometry; these data have the advantage to be naturally available for all our candidates.

The variation of the Ly α rest-frame EW as a function of the UV color does not show any trend (Fig. 4). Insofar as the UV color reflects the continuum extinction, this is consistent with a decoupling of the reddening of line and continuum photons in the resonant scattering process. This is in contrast with the trend reported by Shapley et al. (2003) of the EW increasing when the UV continuum slope becomes bluer. Their trend, however, encompasses a much wider range of EW than ours, from strong absorption to strong emission, and would be less significant if restricted to our actual limited range of EW.

The Ly α rest-frame EW does not reveal any trend either as a function of the UV luminosity (Fig. 5). The deficiency of strong Ly α emissions reported in the most luminous high- z Lyman Break Galaxies (LBGs) (Ando et al. 2004, 2006; Shimasaku et al. 2006) is not directly comparable since it takes place at an absolute magnitude < -21 , a limit that we do not reach in our sample. However, the fraction of objects with large EW is small in Fig. 5 and such objects would likely be missing in a smaller sample of Ly α emitters. This suggests that, in addition to the interpretations given by Ando et al. (2004), the trend seen at high redshift may be due or enhanced by small number statistics.

Fig. 5 allows us also to identify ultra-violet luminous galaxies (UVLGs). This class of galaxies was defined by Heckman et al. (2005) among *GALEX* local galaxies to overlap the luminosity range of typical high- z LBGs. With the actual definition of Heckman et al. (2005) we have 11 UVLGs in our sample at the left of the dotted vertical line in Fig. 5. These UVLGs do not have EW as large as those found in less luminous objects. This is comparable, albeit at lower luminosity, with the trend reported for the high- z LBGs. This may also be explained by small number statistics. Using the UV continuum LF obtained in the redshift range 0.2 – 0.4 by Arnouts et al. (2005), we calculate a density of UVLGs of about 2×10^{-5} Mpc $^{-3}$, predicting about 24 of these objects in the redshift window $0.2 < z < 0.35$ and our 5 fields. With this evaluation, about 33 % (8/24) of the UVLGs have Ly α in emission (with an EW larger than about 20 Å) which is a larger fraction than found above for the general population. Given the luminosity range of the UVLGs and the redshift window, incompleteness cannot explain that difference. In contrast the evaluation of the number of luminous galaxies based on the bright end of the UV luminosity function is uncertain. On the other hand it is possible that a larger UV luminosity may contribute to a larger Ly α escape. This would be consistent, in addition to a possible evolution of the Ly α escape fraction, with the higher incidence of Ly α emission at higher redshifts reported by Reddy et al. (2007) and Ouchi et al. (2007).

3.4. Ly α dependences: corollary information

Galaxy parameters which are not derived from *GALEX* observations are available for only a fraction of our relatively distant objects. An extreme example is the H α line emission which would be interesting in order to get the amount of ionizing radiation without the complication of resonant scattering and, therefore, the Ly α escape fraction. In spite of the 12 spectroscopic redshifts found in the literature (Table 2), we have been unable for various reasons (essentially lack of calibrated fluxes) to recover the H α flux in more than 2 galaxies. The resulting Ly α /H α ratios are found to be 19 (GROTH-21024) much above the theoretical recombination ratio of 8.7 and 5 (GROTH-34512) which is larger than any reported value in near-by star forming galaxies (Giavalisco, Koratkar, & Calzetti 1996). These findings illustrate the difficulties of spectrophotometric comparisons and the need for a dedicated optical spectroscopic follow-up.

The SDSS photometry (u, g, r, i, z filters) is available for three of our five fields and 64 of our Ly α emitting galaxy candidates. We have calculated the (NUV–r) color which has been extensively used by Wyder et al. (2007) in their study of galaxy colors with *GALEX* and is known to make a pronounced demarcation between the blue and red sequences. The range of colors obtained for our Ly α emitting galaxy candidates is in good agreement with the values expected from galaxies. We find no trend between this color and the Ly α rest-frame EW, the Ly α line luminosity and the FUV luminosity. The (u–r) vs. (NUV–r) color-color diagram (Fig. 6) shows a sequence in good agreement with the blue part of the sequence (NUV–r < 4) obtained in the same diagram by Wyder et al. (2007) on a very large sample of galaxies (their figure 22). In contrast the density of galaxies along our sequence is relatively constant whereas it increases in the diagram of Wyder et al. (2007) with the (NUV–r) color increasing from 0 to ~ 3 . This difference results probably from the selection of our objects among star-forming galaxies with a significant far-UV continuum and at redshift $z > 0.2$. We have separated the objects of Fig. 6 into three groups according to their Ly α EW values. These categories do not appear segregated either along or perpendicular to the sequence which is primarily driven, as suggested by Wyder et al. (2007), by star formation history. Since the Ly α EW (without any transfer) is predicted rather stable as a function of time in galaxies with constant star formation (Charlot & Fall 1993), this illustrates the dominant role of individual radiation transfer effects in the Ly α escape rather than the stellar population properties (e.g.) (Schaerer & Verhamme 2008)

4. The Ly α luminosity function

4.1. Volume evaluation and space density

For this approach we need conditions of detection as uniform as possible. We have therefore restricted ourselves to the redshift range 0.2 – 0.35 and have retained only the objects of quality 1 or 2 in order to limit spurious detections. We have used the V/V_{max} method. For each Ly α emitting galaxy candidate, V_{max} is the volume over which a source of the same Ly α luminosity could lie and still meet the blind search criteria. The inverse volumes of all the galaxies in a particular luminosity bin are summed to estimate the luminosity function in that bin.

V_{max} is defined by the field of view and the redshift range 0.2 – z_l . The redshift z_l is 0.35 if the Ly α luminosity is bright enough that the line remains above the line flux limit out to the upper bound of the redshift window. The corresponding volume, maximum value of V_{max} , is $2.369 \times 10^5 \text{ Mpc}^{-3}$ taking into account a 0.6 deg field of view radius. For fainter sources, z_l is the redshift (< 0.35) at which the Ly α flux falls below the line flux limit. In this determination the Ly α flux is decreased as the inverse square of the luminosity distance since the Ly α is not spectrally resolved in the galaxies. The determination of z_l is somewhat uncertain since it is based on the line flux limit which is evaluated empirically in each field and results from both the depth of each field and the continuum level of the spectra. In practice, slight adjustments have been made to account for the specific noise in each spectra. Because of the relatively narrow redshift window, only the sources with a Ly α luminosity less than $10^{42} \text{ erg s}^{-1}$ may be affected by these uncertainties in volume evaluation.

In order to combine the results obtained over the five fields we have to deal with the differences of depth. With the upper redshift limit of 0.35, the sources with Ly α luminosity $\log(L) > 41.8 \text{ (erg s}^{-1}\text{)}$ are essentially above the line flux limits in all fields and can be reasonably merged. Adopting a bin width of 0.2 in $\log(L)$, we have summed up the inverse volumes in their respective bins over the 5 fields and divided by 5 to account for the increased volume. It is possible to get the luminosity function below the limit of $\log(L) = 41.8 \text{ (erg s}^{-1}\text{)}$ at the expense of cosmic variance by using only the deepest three fields, CDFS, GROTH and NGPDWS (cf Table 1). We have repeated the summations of inverse volumes over these three fields. The bin below $\log(L) = 41.6 \text{ (erg s}^{-1}\text{)}$ is again affected by incompleteness and the lowest bin with only one source has been discarded as insignificant.

The resulting luminosity function per \log Ly α luminosity is plotted in Fig. 7. As a generic consequence of detection thresholds in images, the lowest bins of the luminosity function are affected by incompleteness. We have not tried to remedy this type of incompleteness and will only refrain to use the lowest luminosity bins in further discussion.

4.2. Correction for incompleteness

In contrast to the generic incompleteness accompanying the lowest bins of the luminosity function, we have another source of incompleteness attached to the spectroscopic functionality of the grism images. The inclusion of a detected galaxy in the luminosity function depends on the detection of the Ly α line. This source of incompleteness, which has no reasons to be confined to the lowest luminosity bins, can take two aspects. First, a number of features with small equivalent width may be missed by lack of contrast over the continuum flux: the distribution of EWs (similar to the distribution of rest-frame EW in Fig. 3) shows this happens below approximately EW = 20 Å. Second, objects with EW larger than about 20 Å may be missed because their continuum flux is too low for a spectrum to have been extracted: Fig. 2 shows that spectra are not systematically extracted below a FUV magnitude of 21.5.

In order to understand the mechanisms of this second aspect of the incompleteness, we have illustrated the interplay between EW and observed FUV magnitudes in Fig. 8. Because of the limited redshift range, each luminosity bin corresponds to a relatively narrow domain in this diagram. As an example, Fig. 8 shows the domain for the luminosity bin $\log(L_{Ly\alpha})$ 41.8 – 42.0 (erg s^{-1}), between the two curves corresponding to Ly α line fluxes of 1.5 and $8.7 \times 10^{-15} \text{ erg cm}^{-2} \text{ s}^{-1}$. This domain is cut in two by the horizontal continuum flux limit at magnitude 21.5. In order to quantify the incompleteness, we first calculate the number of galaxies per 0.5 mag bin expected in our volume space as a function of UV magnitude. We use the luminosity function obtained with the FUV band of *GALEX* by Arnouts et al. (2005) in the range $0.2 < z < 0.4$. In each 0.5 mag bin the galaxies are in turn distributed in 10 Å EW bins according to the observed EW distribution (above the limit of 20 Å). This results in a number of Ly α emitting galaxies for each elementary cell of size 0.5 mag and 10 Å EW in the diagram of Fig. 8. These galaxy numbers per elementary cell can be summed over the domain defined above in Fig. 8. The incompleteness factor is then taken as the ratio of the sum over the entire domain to the sum over the domain above the limit of 21.5 in magnitude. If we account for the galaxies fainter than 21.5 already contributing to the space densities plotted in Fig. 7, we end up with an incompleteness factor of 6 for the Ly α luminosity bin 41.8 – 42.0 ($\log \text{erg s}^{-1}$) taken as example in Fig. 8.

We emphasize this correction factor does not result from simulated data but only from an evaluation using the FUV luminosity function and relying on the assumption that the observed EW distribution of galaxies apply to the less luminous galaxies involved in the evaluation. This assumption is supported by two facts. First, the observed EW distribution does not seem to change as a function of the UV luminosity (Fig. 5) at least in the observed range of luminosity. Second, the bulk of the correction factor originates from galaxies 1

or 1.5 mag fainter than the 21.5 limit with EWs between 40 and 60 Å. This range of EW values seems less prone to change with luminosity than extreme values. As the uncertainties on the correction factor remain severe and the amplitude of the correction is increasing for the low luminosity bins, we have repeated the evaluation only for the three luminosity bins brighter than (41.8 – 42.), finding correction factors of 4.2, 2.6, and 2.7 respectively. The brightest bin, corresponding to just one object, has not been corrected for. The space densities resulting from the incompleteness correction are plotted in Fig. 7.

Fig. 8 can also illustrate the other source of incompleteness resulting from small EW features undetected by lack of contrast over the continuum; the relevant objects would lie in the domain defined by the two lines and the limit at $EW < 20$ Å. The EW distribution is essentially unknown in this area but, for all reasonable assumptions, an evaluation based on the same scheme as above leads to a negligible additional factor. This is due to the fact that galaxies are bright in this domain (at least those related to the high luminosity bins) and consequently much less dense than the faint galaxies involved in the first source of incompleteness described above.

4.3. Comparisons with H α luminosity functions

In the same way as the comparison of the Ly α luminosity with the H α luminosity of an individual star-forming galaxy places constraints on the escape of Ly α photons through the resonant scattering process, we may compare the Ly α and the H α luminosity functions of galaxies. Since the escape of Ly α emission is expected to be highly variable from galaxy to galaxy, the comparison will lead to an average (Ly α flux weighted) value of the escape, as if all galaxies were the same. For this comparison we have used the H α luminosity function of Tresse & Maddox (1998) obtained at $z \sim 0.2$, close to our redshift window. This luminosity function is itself consistent with other determinations (Tresse et al. 2002; Fujita et al. 2003; Nakamura et al. 2004). We adopt the values $\log(L^*) = 41.92$ ergs s $^{-1}$ and $\log(\Phi^*) = -2.56$ Mpc $^{-3}$ as updated from Tresse & Maddox (1998) to current cosmology ($H_0 = 70$ km s $^{-1}$ Mpc $^{-1}$, $\Omega_\Lambda = 0.7$, $\Omega_m = 0.3$) by Fujita et al. (2003).

Because our binned data points are few and related to high luminosity values, we assume for our Ly α luminosity function the same value $\alpha = -1.35$ as determined for the H α LF. The Ly α /H α ratio and the fraction of galaxies with Ly α emission are directly given by the factor of modifications of the parameters L^* and Φ^* to fit our Ly α data. A change of L^* alone does not work well (see one example in Fig. 7) and a reasonable fit requires to decrease Φ^* , or, as currently observed, to have Ly α in emission in only a fraction of the galaxies. Although systematic errors may be present in our completeness correction, we

have carried out a least-square fit on the 5 brightest luminosity data with L^* and Φ^* as free parameters. The fit (Fig. 7), given by $\log(L^*) = 41.98 \pm 0.09$ ergs s^{-1} and $\log(\Phi^*) = -3.40 \pm 0.16$ Mpc^{-3} , implies a $\text{Ly}\alpha/\text{H}\alpha$ ratio of about 1 in 15 % of the galaxies. As expected, the $\text{Ly}\alpha/\text{H}\alpha$ ratio is much lower than the ratio of 8.7 predicted by the case B recombination theory. This is in rough agreement with the range of values reported in nearby galaxies by Giavalisco, Koratkar, & Calzetti (1996). This implies an average $\text{Ly}\alpha$ escape fraction of about 0.1 somewhere between the average values of 0.02 and 0.8 in the galaxy formation models of Le Delliou et al. (2006) and Kobayashi, Totani, & Nagashima (2007) respectively.

At this stage, it is also possible to show that the $\text{Ly}\alpha$ luminosity function is not affected by the fact that we have been unable to distinguish and remove narrow-line AGNs from our sample of $\text{Ly}\alpha$ emitting galaxy candidates. We use the $\text{H}\alpha$ luminosity function of narrow-line AGNs derived from the SDSS by Hao et al. (2005b) with the criterion of Kauffmann et al. (2003) which gives the largest number of objects. The $\text{Ly}\alpha$ LF is derived with the $\text{Ly}\alpha/\text{H}\alpha$ ratio of 3.24 reported by Vanden Berk et al. (2001) from SDSS composite quasar spectra. The plot in Fig. 7 shows that the contribution of narrow-line AGNs remains small even if we account for some evolution between the redshift window of the SDSS sample (0 - 0.15) and ours (0.2 - 0.35).

4.4. Comparisons with $\text{Ly}\alpha$ luminosity functions at high z

The space densities of *GALEX* $\text{Ly}\alpha$ emitting galaxies at $0.2 < z < 0.35$ are interesting to compare with the $\text{Ly}\alpha$ LFs found at high redshift. In Fig. 9 we have first plotted the $\text{Ly}\alpha$ LF obtained by van Breukelen, Jarvis, & Venemans (2005) at redshifts $2.3 < z < 4.6$ which is selected because it is the closest from our data in terms of redshift. In addition, the authors have compared their data with the measurements available at the time (references therein and their Figure 5). They conclude that the luminosity function of $\text{Ly}\alpha$ emitters does not significantly change from $z \sim 3.4$ to $z = 5.7$. This is confirmed by more recent determinations from Ajiki et al. (2006), Tapken et al. (2006), Shimasaku et al. (2006), Murayama et al. (2007), Gronwall et al. (2007), Ouchi et al. (2007) and Dawson et al. (2007). A few LFs at $z > 6$ have been left out of the comparison because variations of $\text{Ly}\alpha$ LFs are possible that would not be related to the galaxies themselves but to the IGM opacity resulting from changes in the IGM neutral fraction accompanying the re-ionisation. Of the recent $\text{Ly}\alpha$ LFs at high redshift, we have elected for clarity to reproduce in Fig. 9 only those closest from our redshift range, i.e. the two from Gronwall et al. (2007) and Ouchi et al. (2007) at $z = 3.1$.

Fig. 9 shows that the space density of the $\text{Ly}\alpha$ emitting galaxies is much lower in the range $0.2 < z < 0.35$ than at redshifts about 3. We have quantified this factor

by a least-square fit on the 5 brightest data points, using the same α parameter (-1.6) as van Breukelen, Jarvis, & Venemans (2005) (adopted by these authors from Steidel et al. (1999)); we have obtained $\log(L^*) = 42.03 \pm 0.08 \text{ ergs s}^{-1}$ and $\log(\Phi^*) = -3.47 \pm 0.17 \text{ Mpc}^{-3}$.

By comparison with the values $L^* = 5 \pm 1.8 \times 10^{42} \text{ ergs s}^{-1}$ and $\Phi^* = 0.0012 \pm 0.0005 \text{ Mpc}^{-3}$ of van Breukelen, Jarvis, & Venemans (2005), our determination implies a Ly α luminosity density (LD) ~ 16.5 times larger at $z \sim 3$ than at $0.2 < z < 0.35$. In comparison, the FUV LD of Schiminovich et al. (2005) increases by a factor of about 5 between $z = 0.3$ and $z \sim 3$, an increase consistent with the compilations of SFR evolution of Hopkins (2004) and Hopkins & Beacom (2006). We have illustrated this difference in the evolution rates of the FUV and Ly α luminosity densities in Fig. 9 by plotting the effect of a factor 5 decrease of the parameters L^* or Φ^* of the LF of van Breukelen, Jarvis, & Venemans (2005). Although the effect looks significant, we discuss further the uncertainties in our approach as well as possible interpretations.

1) Insofar as the FUV LD measures the evolution of the massive stellar content of the galaxies, the faster rate of evolution of the Ly α LD suggests a real increase (by a factor of about 3) of the Ly α escape fraction from $z \sim 0.3$ to $z \sim 3$. This is consistent with the observations of an increase with redshift of the fraction of ($\text{EW} > 20$) Ly α emitting galaxies (this paper, Reddy et al. (2007)). This is also consistent with the current idea that galactic winds are increasing with redshift, favouring the Ly α escape while mitigating the increased fraction of neutral hydrogen in galaxies at high redshift.

2) The rate of increase of the Ly α LD between $z = 0.3$ and $z \sim 3$ depends on the uncertainties of L^* and Φ^* at both redshifts, i.e. 4 parameters. If we combine the variances obtained from our least-square fit with those given by van Breukelen, Jarvis, & Venemans (2005), the standard deviation on the factor 16.5 is as large as 11.5 and the evolution of the Ly α LD is faster than the FUV LD at a significance of about 84%.

3) A change in the faint-end slope α of the LF may play a role in the evolution of the Ly α LD which writes as $L^*\Phi^*\Gamma(\alpha+2)$. The parameter α is indeed poorly constrained by the space densities of the luminous Ly α emitters that are observed both by *GALEX* and at high redshift. This parameter is assumed to be the same in our comparison between low and high redshifts. A steepening of the slope α at low z , resulting in an increase of $\Gamma(\alpha+2)$ could make the evolution of the Ly α LD matching that of the FUV LD. This would mean an increase of the Ly α escape fraction in low-luminosity objects at low z . Such a variation, however, would be opposite to the current trend of a steepening of the faint-end slope with redshift (e.g. Ryan et al. (2007) for FUV LF) as expected in the hierarchical formation scenario of galaxies.

In conclusion, the faster rate of evolution of the Ly α luminosity density with respect to the cosmic star formation rate is significant at about 84% and indicates probably an increase of the average Ly α escape fraction from $z \sim 0.3$ to $z \sim 3$.

5. Conclusion

A blind search of potential Ly α emission features has been conducted on 7018 spectra obtained in 5 deep spectroscopic exposures with *GALEX*. 96 Ly α emitting galaxy candidates are identified, after a separation from AGNs essentially on the basis of the FWHM. They are mostly in the redshift range (0.2 – 0.35). The following properties stand out:

1) The Ly α rest frame equivalent width distribution is comparable with that reported by Shapley et al. (2003) for LBGs at $z \sim 3$. The fraction of galaxies with Ly α emission (EW > 20 Å) seems smaller, 15% against 25% in the LBG sample.

2) No trend is found between the EW and the (FUV – NUV) color, in agreement with a decoupling of the reddening of line and continuum photons in Ly α resonant scattering. There is no trend either of the EW with the UV luminosity, except a decrease in a sub-sample of ultra-violet luminous galaxies (UVLGs). As at very high-redshifts, small-number statistics might play a role here. A larger fraction of Ly α emitting galaxies (EW > 20 Å) is found among UVLGs.

3) A sub-sample of 66 emission features of better quality and strictly in the redshift range (0.2 – 0.35) has been used to calculate the space densities of the Ly α emitting galaxies. A scheme has been presented to correct for a major source of incompleteness, the fact that spectra of objects with significant EW may have not been extracted because their continuum is too weak.

4) A comparison with the H α luminosity function of Tresse & Maddox (1998) in the same redshift domain is consistent with an average Ly α to H α ratio of 1 in about 15% of the galaxies.

5) A comparison of the Ly α luminosity functions at $z \sim 0.3$ and $z \sim 3$ shows an evolution beyond that expected from the evolution of the massive stellar content of star-forming galaxies at a significance level of 84%, suggesting a increase of the average Ly α escape fraction with redshift.

GALEX (*Galaxy Evolution Explorer*) is a NASA Small Explorer, launched in April 2003. We gratefully acknowledge NASA's support for construction, operation, and science

analysis for the *GALEX* mission, developed in cooperation with the Centre National d'Etudes Spatiales of France and the Korean Ministry of Science and Technology. This research has made use of the NASA/IPAC Extragalactic Database (NED) which is operated by the Jet Propulsion Laboratory, California Institute of Technology, under contract with the National Aeronautics and Space Administration.

REFERENCES

- Ahn, S.-H., Lee, H.-W., & Lee, H. M. 2001, *ApJ*, 554, 604
- Ahn, S.-H., Lee, H.-W., & Lee, H. M. 2002, *ApJ*, 567, 922
- Ahn, S.-H., Lee, H.-W., & Lee, H. M. 2003, *MNRAS*, 340, 863
- Ajiki, M., Mobasher, B., Taniguchi, Y. et al., 2006, *ApJ*, 638, 596
- Ando, M., Ohta, K., Iwata, I. et al., 2004, *ApJ*, 610, 635
- Ando, M., Ohta, K., Iwata, I. et al., 2006, *ApJ*, 645, 19
- Arnouts, S., Schiminovich, D., Ilbert, O. et al., 2005, *ApJ*, 619, L43
- Charlot, S., & Fall, S. M. 1993, *ApJ*, 415, 580
- Chen, W. L., & Neufeld, D. A. 1994, *ApJ*, 432, 567
- Cowie, L. L., & Hu, E. M. 1998, *AJ*, 115, 1319
- Davis, M., Guhathakurta, P., Konidaris, N. P. et al. 2007, *ApJ*, 660, L1
- Dawson, S., Rhoads, J. E., Malhotra, S. et al. 2007, *ApJ*, 671, 1227
- Djorgovski, S., & Thompson, D. J. 1992, in *The Stellar Populations of Galaxies*, IAU Symp. 149, ed. B. Barbuy & A. Renzini, p 337
- Finkelstein, S. L., Rhoads, J. E., Malhotra, S., Pirzkal, N., & Wang, J. 2007, *ApJ*, 660, 1023
- Fujita, S. S., Ajiki, M., Shioya, Y. et al., 2003, *ApJ*, 586, L115
- Giavalisco, M., Koratkar, A., & Calzetti, D. 1996, *ApJ*, 466, 831
- Gronwall, C., Ciardullo, R., Hickey, T. et al. 2007, *ApJ*, 667, 79
- Haiman, Z. 2002, *ApJ*, 576, L1

- Hansen, M., & Oh, S. P. 2006, MNRAS, 367, 979
- Hao, L., Strauss, M. A., Tremonti, C. A. et al., 2005, AJ, 129, 1783
- Hao, L., Strauss, M. A., Fan, X. et al., 2005, AJ, 129, 1795
- Heckman, T. M., Hoopes, C. G., Seibert, M. et al., 2005, ApJ, 619, L35
- Hopkins, A. M. 2004, ApJ, 615, 209
- Hopkins, A. M., & Beacom, J. F. 2006, ApJ, 651, 142
- Hu, E. M., Cowie, L. L., & McMahon, R. G. 1998, ApJ, 502, 99
- Kashikawa, N., Shimasaku, K., Malkan, M. A. et al. 2006, ApJ, 648, 7
- Kauffmann, G., Heckman, T. M., Tremonti, C. et al. 2003, MNRAS, 346, 1055
- Kennicutt, R. C. 1998, ARA&A, 36, 189
- Kobayashi, M. A. R., Totani, T., & Nagashima, M. 2007, ApJ, 670, 919
- Kunth, D., Mas-Hesse, J. M., Terlevich, E. et al., 1998, A&A, 334, 11
- Le Delliou, M., Lacey, C. G., Baugh, C. M., & Morris, S. L. 2006, MNRAS, 365, 712
- Malhotra, S. & Rhoads, J. E. 2004, ApJ, 617, L5
- Martin, D.C., Fanson, J., Schiminovich, D. et al., 2005, ApJ, 619, L1
- Mas-Hesse, J. M., Kunth, D., Tenorio-Tagle, G. et al., 2003, ApJ, 598, 858
- Morrissey, P., Schiminovich, D., Barlow, T.A. et al., 2005, ApJ, 619, L7
- Morrissey, P., Conrow, T., Barlow, T.A. et al., 2007, ApJS, 173, 682
- Murayama, T., Taniguchi, Y., Scoville, N. Z. et al. 2007, ApJS, 172, 523
- Nakamura, O., Fukugita, M., Brinkmann, J., & Schneider, D. P. 2004, AJ, 127, 2511
- Neufeld, D. A. 1991, ApJ, 370, L85
- Ouchi, M., Shimasaku, K., Furusawa, H. et al. 2003, ApJ, 582, 600
- Ouchi, M., Shimasaku, K., Akiyama, M. et al. 2007, astro-ph/ 07073161

- Pettini, M., Kellogg, M., Steidel, C. C., Dickinson, M., Adelberger, K. L., & Giavalisco, M., 1998, *ApJ*, 508, 539
- Pettini, M., Steidel, C. C., Adelberger, K. L., Dickinson, M., & Giavalisco, M., 2000, *ApJ*, 528, 96
- Reddy, N. A., Steidel, C. C., Pettini, M. et al. 2007, astro-ph/07064091
- Ryan, R. E., Hathi, N. P., Cohen, S. H. et al. 2007, *ApJ*, 668, 839
- Schaerer, D. 2007, IAC Winterschool, Lecture on Primeval Galaxies, astro-ph/0706.0139
- Schaerer, D. & Verhamme, A. 2008, astro-ph/0801.1187
- Schiminovich, D., Ilbert, O., Arnouts, S. et al., 2005, *ApJ*, 619, L47
- Shapley, A. E., Steidel, C. C., Pettini, M., & Adelberger, K. L. 2003, *ApJ*, 588, 65
- Shectman, S. A., Landy, S. D., Oemler, A. et al., 1996, *ApJ*, 470, 172
- Shimasaku, K., Kashikawa, N., Doi, M. et al. 2006, *PASJ*, 58, 313
- Stanway, E. R., Bunker, A. J., Glazebrook, K. et al. 2007, *MNRAS*, 376, 727
- Steidel, C. C., Adelberger, K. L., Giavalisco, M., Dickinson, M., & Pettini, M. 1999, *ApJ*, 519, 1
- Stern, D., Yost, S. A., Eckart, M. E. et al., 2005, *ApJ*, 619, 12
- Tapken, C., Appenzeller, I., Gabasch, A. et al., 2006, *A&A*, 455, 145
- Tresse, L., & Maddox, S. J. 1998, *ApJ*, 495, 691
- Tresse, L., Maddox, S. J., Le Fèvre, O., & Cuby, J.-G. 2002, *MNRAS*, 337, 369
- van Breukelen, C., Jarvis, M. J., & Venemans, B. P. 2005, *MNRAS*, 359, 895
- Vanden Berk, D. E., Richards, G. T., Bauer, A. et al., 2001, *AJ*, 122, 549
- Vanzella, E., Cristiani, S., Dickinson, M. et al., 2006, *A&A*, 454, 423
- Verhamme, A., Schaerer, D., & Maselli, A. et al. 2006, *A&A*, 460, 397
- Way, M. J., Quintana, H., Infante, D. G. et al., 2005, *AJ*, 130, 2012
- Weiner, B. J., Phillips, A. C., Faber, S. M. et al., 2006, *ApJ*, 620, 595

Wyder, T. K., Martin, D. C., Schiminovich, D. et al., 2007, *ApJS*, 173, 293

Wolf, C., Meisenheimer, K., Kleinheinrich, M. et al., 2004, *A&A*, 421, 913

Xu, C.K., Donas, J., Arnouts, S. et al., 2005, *ApJ*, 619, L11

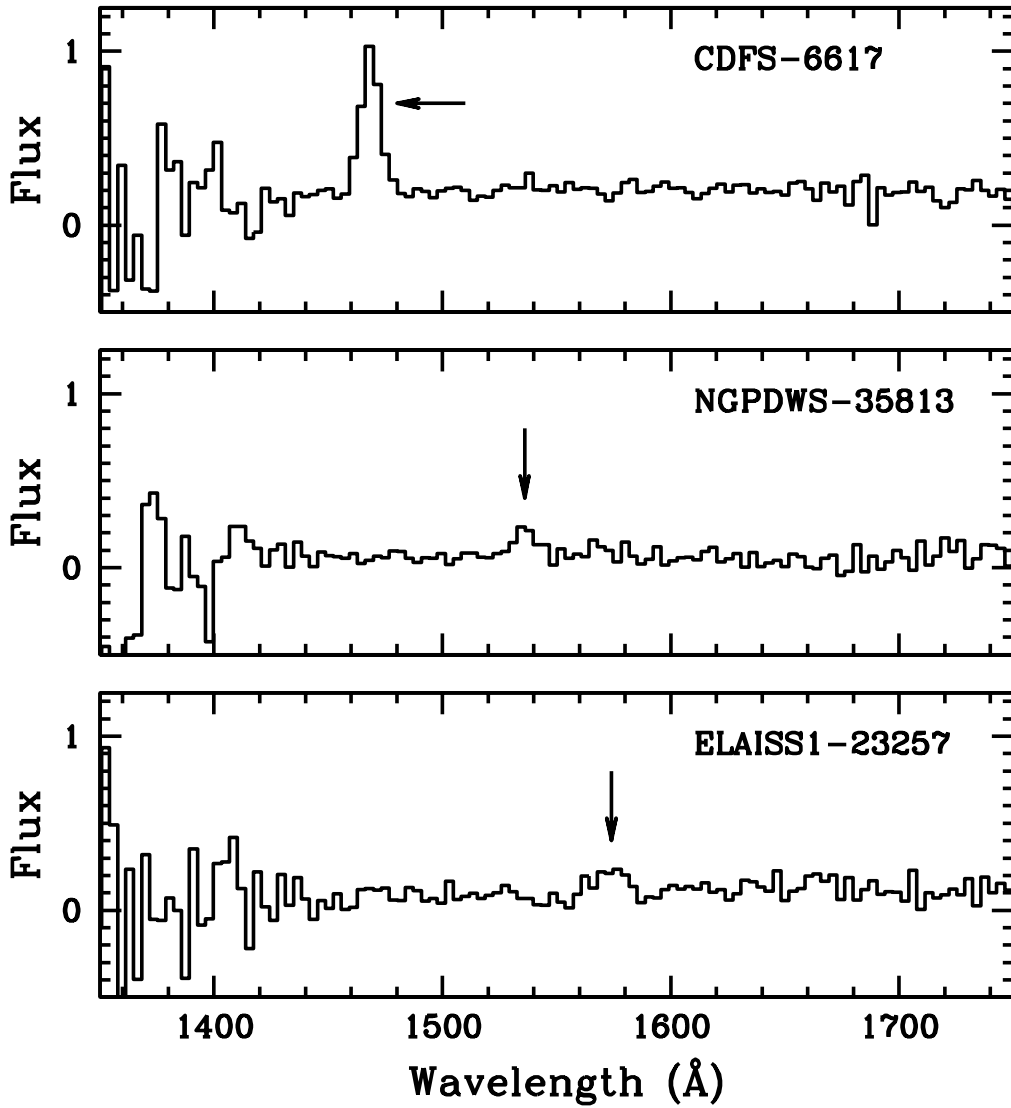


Fig. 1.— Examples of *GALEX* spectra (in 10^{-4} photons cm^{-2} s^{-1} \AA^{-1} flux unit) and features identified as Ly α emission with qualities good ($Q = 1$), fair ($Q = 2$), uncertain ($Q = 3$) from top to bottom.

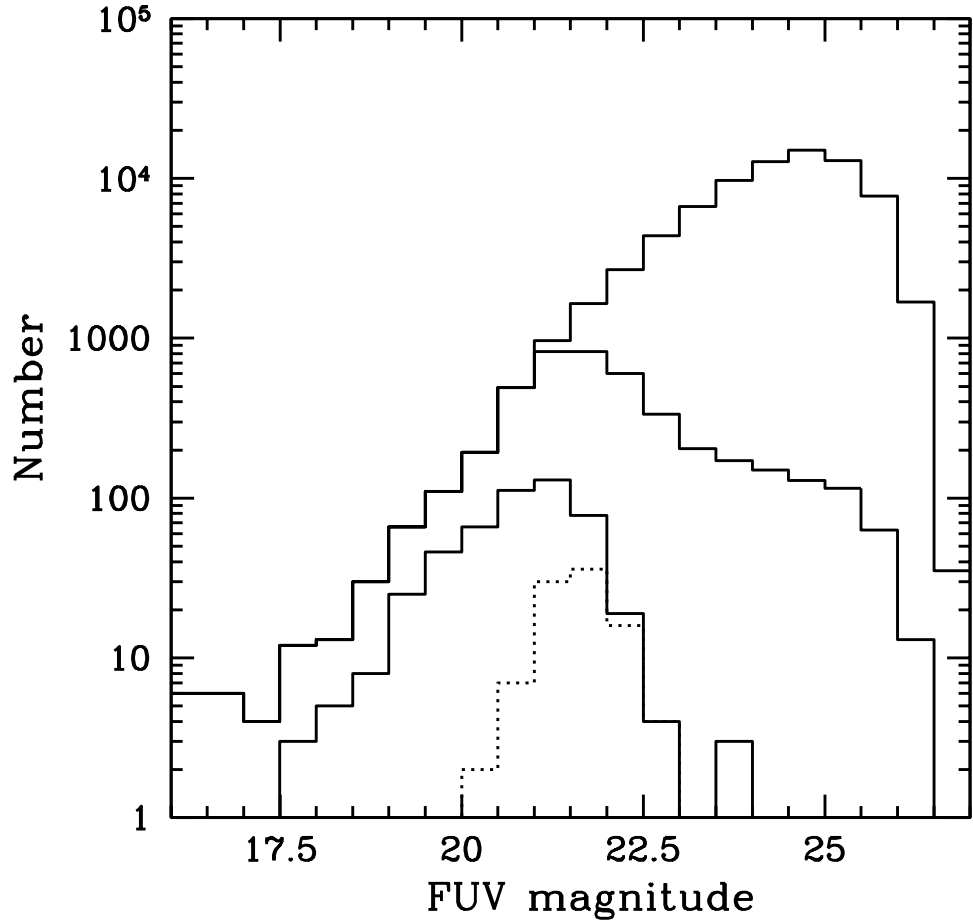


Fig. 2.— Distribution of FUV (AB)magnitudes (all five fields selected). From top to bottom (solid line) sources detected in the images, sources with an extracted spectrum and sources classified as galaxies. The dotted line is for the Ly α emitting galaxy candidates.

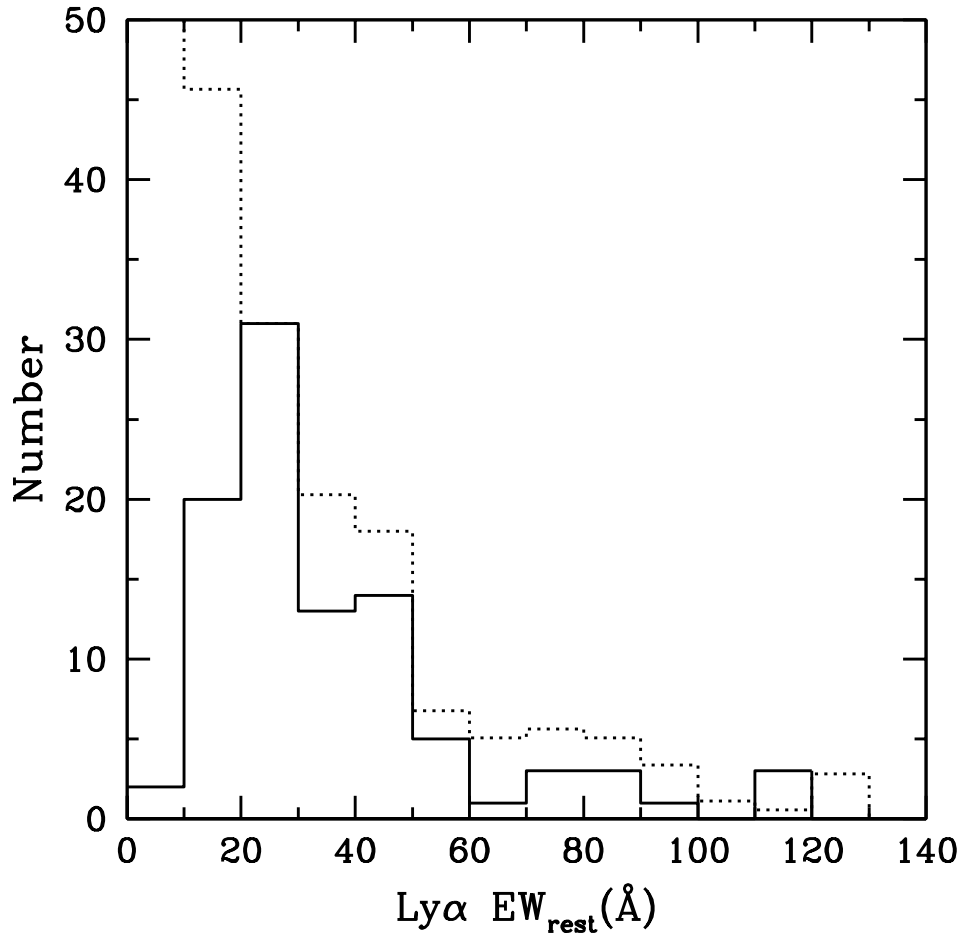


Fig. 3.— Distribution of Ly α rest-frame equivalent width (EW). The distribution of Shapley et al. (2003) is shown (dotted line) after a normalisation with our data in the 20–30 Å bin.

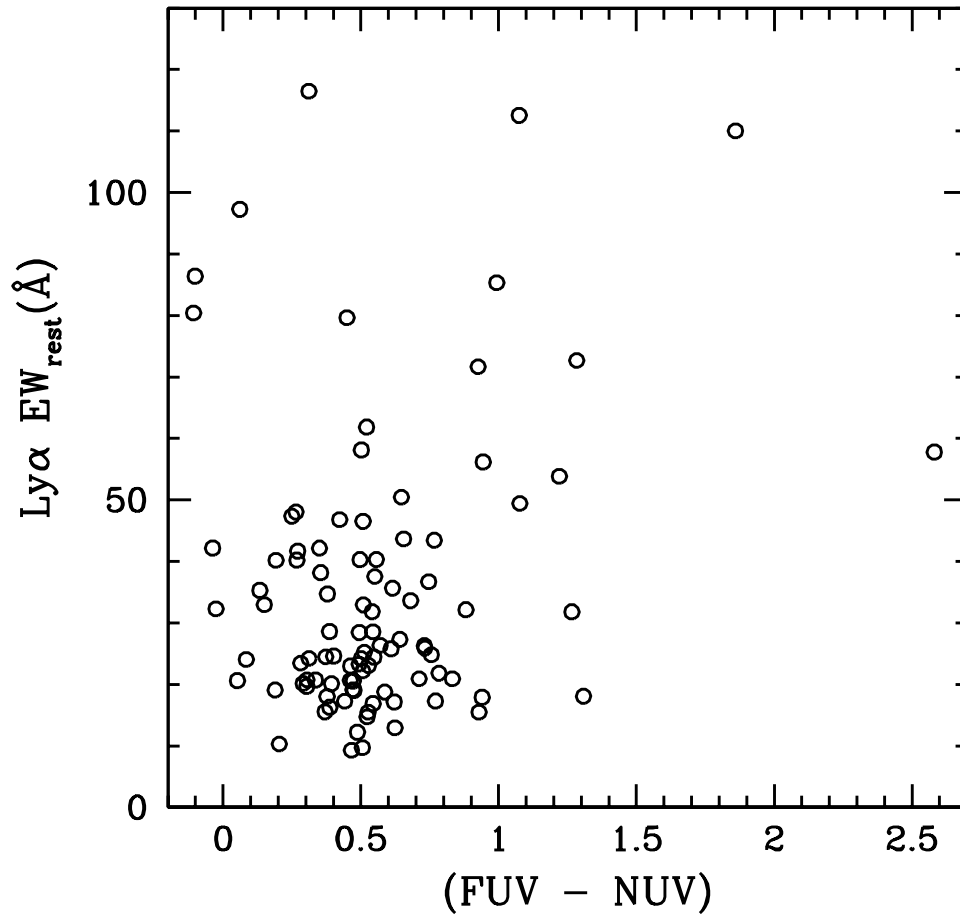


Fig. 4.— Ly α rest-frame EW as a function of the (FUV–NUV) color.

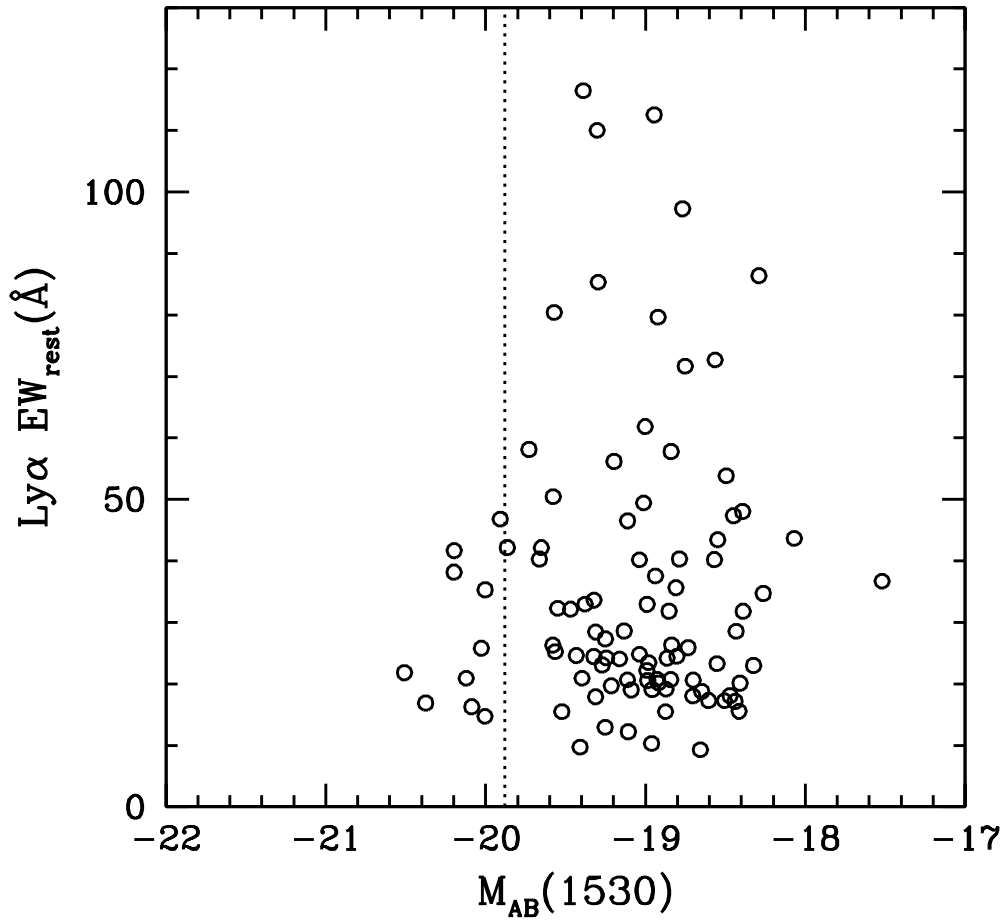


Fig. 5.— Ly α rest-frame EW as a function of the FUV absolute magnitude. The objects brighter than -19.9 (vertical dotted line) are UVLGs according to the definition of Heckman et al. (2005). The high-redshift galaxies discussed by Ando et al. (2004) are also at the left of this line.

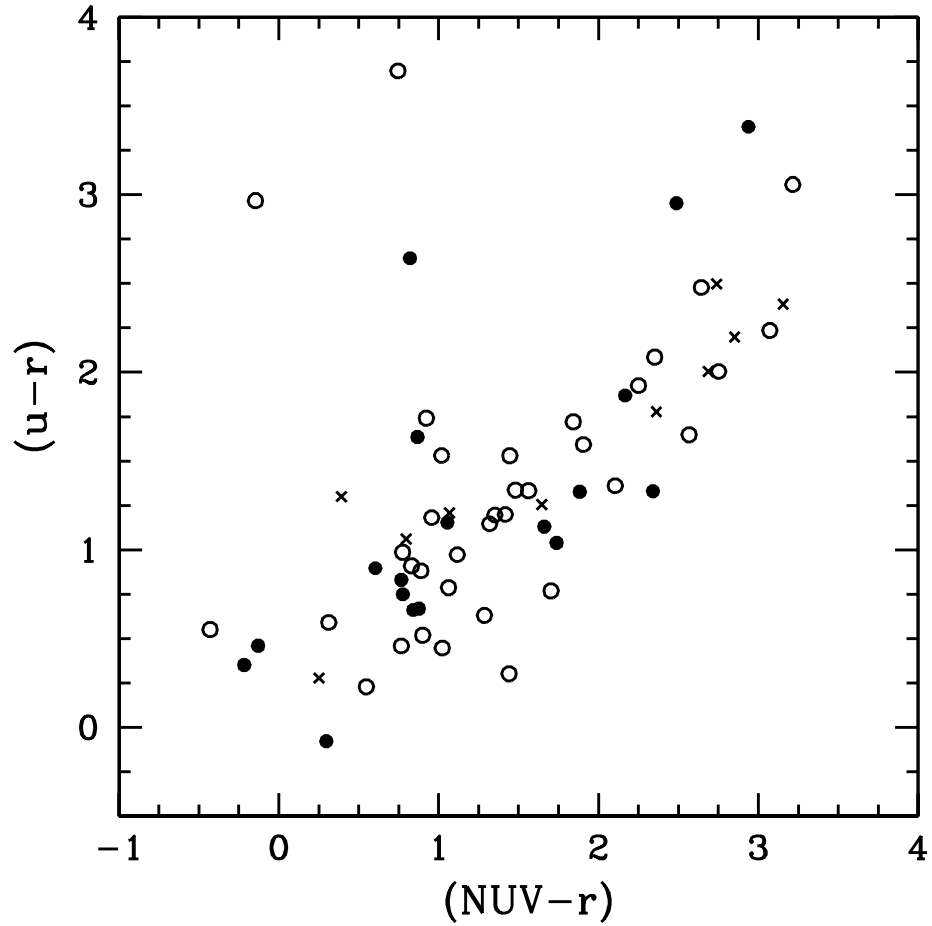


Fig. 6.— $(u-r)$ vs. $(NUV-r)$ color-color diagram built with the *GALEX* NUV flux and the SDSS flux measurements available for 64 of our $\text{Ly}\alpha$ emitting galaxy candidates. One candidate with a low quality emission feature and a $(u-r)$ color of about 6 out of the range expected from galaxies has been discarded. Different symbols are used according to the $\text{Ly}\alpha$ rest-frame EW: $\text{EW} < 30 \text{ \AA}$ (open circle), $30 < \text{EW} < 50 \text{ \AA}$ (solid circle), $\text{EW} > 50 \text{ \AA}$ (crosses).

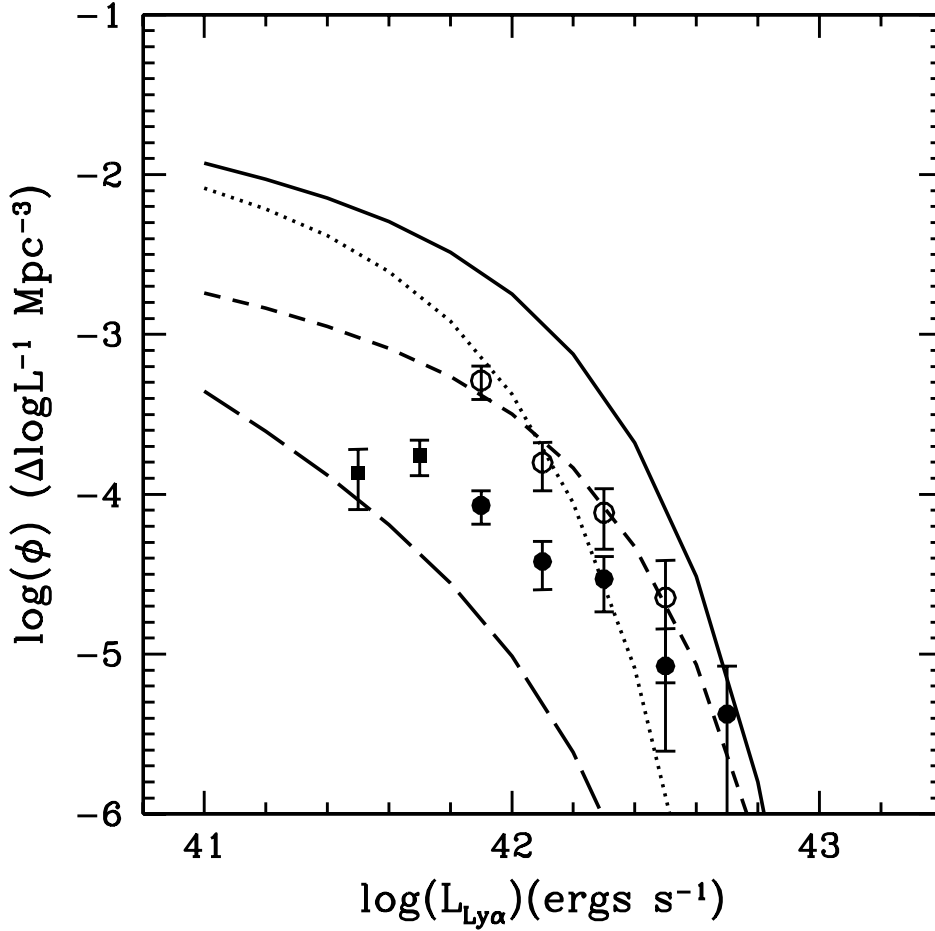


Fig. 7.— The space density of Ly α emitting galaxies ($0.2 < z < 0.35$) per log Ly α luminosity: as measured (solid circles: all five fields, solid squares: CDFS, GROTH and NGPDWS fields), with an evaluation accounting for incompleteness (open circles). The error bars are Poisson errors in our bins. Luminosity functions derived from the H α luminosity function of Tresse & Maddox (1998) are shown with Ly α /H α = 1 for all galaxies (solid line); Ly α /H α = 0.5 for all galaxies (dotted line); and a least-square fit close to Ly α /H α = 1 in 15 % of galaxies (short-dashed). An evaluation of the Ly α luminosity function of narrow-line AGNs, derived from the H α luminosity function of Hao et al. (2005b) is displayed (long-dashed) for comparison.

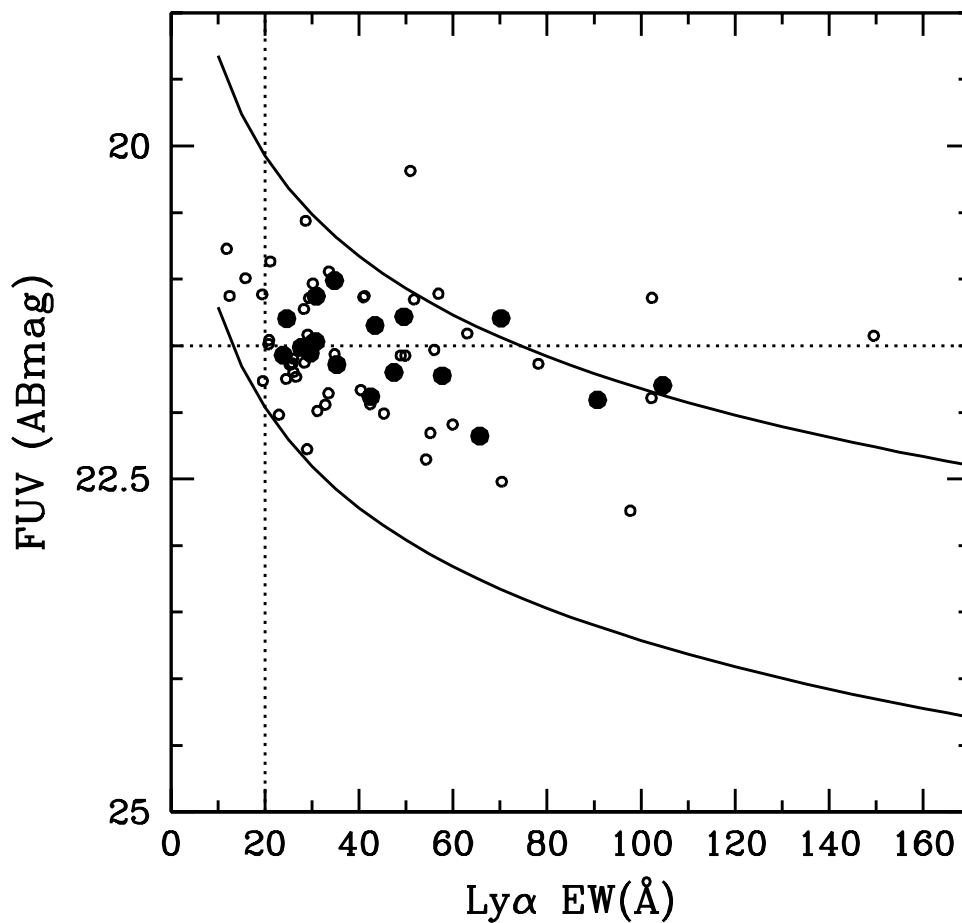


Fig. 8.— The FUV (AB mag) flux vs. the Ly α equivalent width. The objects from the Ly α luminosity bin 41.8 - 42.0 ($\log(\text{Ly}\alpha)$ in ergs s^{-1}) lie between the two diagonal curves. In this domain, objects below the horizontal line at mag 21.5 may be missed because their continuum is too weak and their spectra not extracted; objects at the left of the vertical line may be missed because of a lack of contrast over the continuum. An evaluation of the resulting incompleteness is described in section 4.2. The observed data are overlaid (circles); the filled circles are the 18 objects of the luminosity bin 41.8 – 42.0. Two of these objects are slightly off the domain because of the average calibration factor involved into the calculation of their Ly α luminosity.

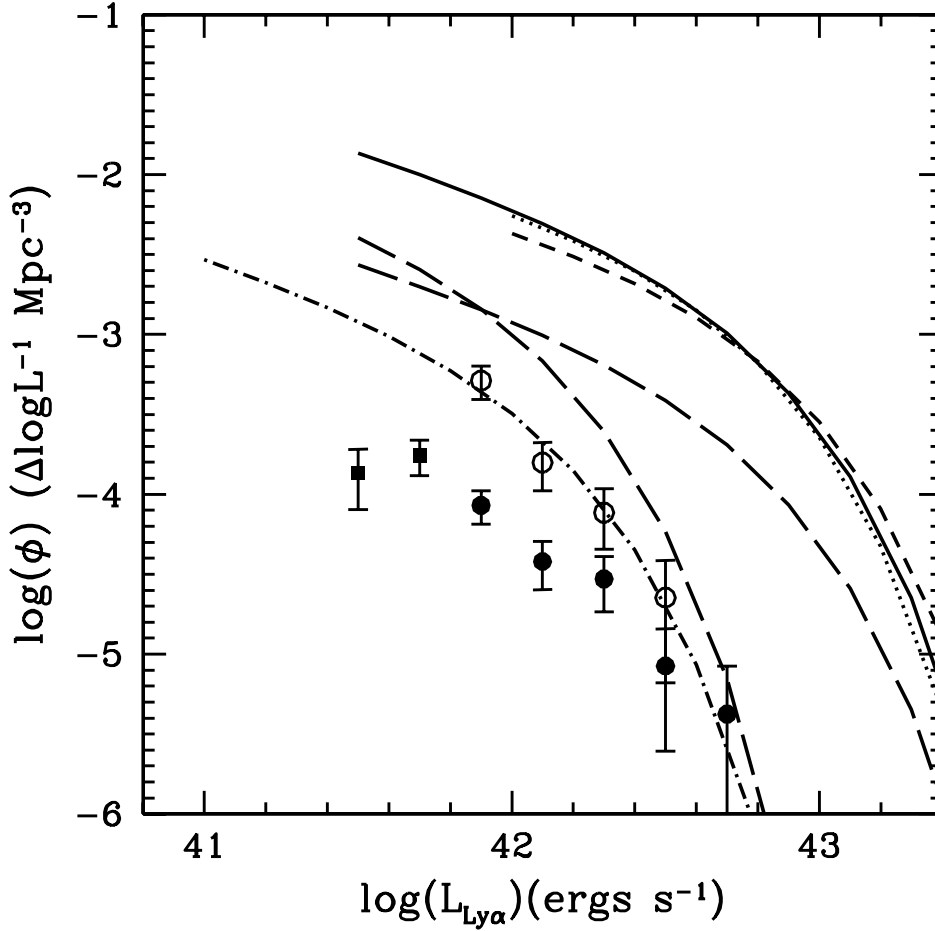


Fig. 9.— The space density of Ly α emitting galaxies ($0.2 < z < 0.35$) per log Ly α luminosity: as measured (solid circles: all five fields, solid squares: CDFS, GROTH and NGPDWS fields), with an evaluation accounting for incompleteness (open circles). Comparison with Ly α luminosity functions at high redshifts: solid line, van Breukelen, Jarvis, & Venemans (2005) at $2.3 < z < 4.6$ ($L^* = 5 \times 10^{42}$ ergs s $^{-1}$, $\Phi^* = 0.0012$ Mpc $^{-3}$, $\alpha = -1.6$); dotted line, Gronwall et al. (2007) at $z \sim 3.1$; short-dashed line, Ouchi et al. (2007) at $z \sim 3.1$. The dot-dashed LF is derived from a least-square fit on the 5 brightest points. The long-dashed lines show the impact of a factor 5 decrease of L^* (the nearest curve to the data points) or Φ^* in the LF of van Breukelen, Jarvis, & Venemans (2005), this factor corresponding to the decrease of the UV luminosity density from $z \sim 3$ to $z \sim 0.3$.

Table 1: Characteristics of the five *GALEX* spectroscopic fields used.

	CDFS-00	ELAISS1-00	GROTH-00	NGPDWS-00	SIRTF-00
Exposure time (s)	149315	84086	281713	139598	79616
Center of field RA ^a	53.128	9.638	214.992	219.156	259.124
Center of field DEC ^a	-27.871	-43.990	52.782	35.171	59.909
Identified sources ^b	38697	30129	43545	40619	28306
Extracted spectra	1419	925	2028	1202	1444
Emission features	22	9	39	19	7
Used for the LF ^c	15	5	29	11	6

^ain decimal degrees.

^bentries in the matched catalog of the FUV and NUV images.

^cused for the evaluation of the luminosity function

Table 2. The Ly α emitting galaxy candidates

Field (1)	ID (2)	RA (3)	DEC (4)	EW (5)	Q (6)	Ly α Flux (7)	FUV (8)	COLOR (9)	z (10)	L(Ly α) (11)	z0 (12)
CDFS	1348	53.2405	-28.3883	43.4	1	5.43	21.35	0.615	0.217	41.87	
CDFS	1821	53.2585	-28.3577	24.6	1	3.37	21.30	0.303	0.251	41.81	
CDFS	2422	52.8947	-28.3395	14.4	2	4.79	20.54	0.488	0.176	41.63	0.1728(1)
CDFS	3801	52.7375	-28.2794	29.7	1	3.62	21.55	0.528	0.285	41.97	
CDFS	4927	52.9765	-28.2386	102.	1	8.12	21.89	0.450	0.283	42.31	
CDFS	5007	53.5412	-28.2554	97.7	2	3.14	22.74	1.283	0.344	42.09	
CDFS	5448	53.0780	-28.2224	149.	1	11.4	21.42	0.312	0.283	42.46	
CDFS	6523	53.0616	-28.1865	47.4	1	3.48	21.70	0.551	0.264	41.87	
CDFS	6535	52.9622	-28.1890	34.8	1	5.16	21.01	0.386	0.216	41.85	
CDFS	6617	53.1743	-28.1903	50.9	1	17.2	20.19	-0.037	0.208	42.33	
CDFS	7100	52.9993	-28.1644	29.1	1	2.96	21.42	0.282	0.239	41.71	
CDFS	10526	53.5868	-28.0657	24.3	1	1.75	22.11	0.940	0.361	41.89	
CDFS	10937	53.7850	-28.0454	63.0	1	5.89	21.41	0.423	0.346	42.37	
CDFS	11518	53.0498	-28.0250	57.7	1	5.50	21.72	0.249	0.218	41.89	0.212(2)
CDFS	16104	53.2360	-27.8879	23.2	2	4.35	21.14	0.544	0.374	42.32	0.365(3)
CDFS	17033	52.7601	-27.8584	38.1	3	3.57	21.96	0.494	0.340	42.14	
CDFS	18142	52.8861	-27.8344	24.4	2	4.63	21.04	0.052	0.183	41.64	0.133(2)
CDFS	19355	53.7296	-27.8008	28.7	1	7.49	20.56	0.783	0.314	42.38	
CDFS	21667	53.2803	-27.7424	11.8	2	2.50	20.77	0.506	0.219	41.55	0.216(4)
CDFS	21739	53.7113	-27.7293	34.8	1	4.05	21.56	0.731	0.323	42.14	
CDFS	30899	53.3592	-27.4543	78.6	1	7.29	21.63	0.502	0.352	42.48	
CDFS	33311	53.1045	-27.2904	58.0	1	8.65	21.43	0.271	0.391	42.66	
ELAISS1	13715	9.6383	-44.0090	21.9	3	2.93	21.64	1.308	0.213	41.59	
ELAISS1	16998	9.5205	-43.8745	56.9	1	8.16	21.11	0.508	0.223	42.08	
ELAISS1	6587	9.5590	-44.2436	102.	1	17.9	21.14	-0.107	0.272	42.62	
ELAISS1	8180	9.8839	-44.1917	38.2	2	10.1	20.34	0.881	0.188	42.01	0.1862(5)
ELAISS1	21062	9.6663	-43.7225	12.5	2	2.81	21.13	0.204	0.211	41.56	
ELAISS1	23257	9.4752	-43.6410	32.7	3	5.17	21.34	0.512	0.294	42.15	
ELAISS1	23425	9.3711	-43.6356	21.1	2	6.49	20.87	0.387	0.300	42.27	
ELAISS1	16921	10.2733	-43.8748	20.3	3	4.14	21.53	0.929	0.312	42.12	
ELAISS1	2386	10.0078	-44.4288	32.8	2	2.81	21.94	0.732	0.268	41.80	
GROTH	6834	215.6564	52.4520	11.1	2	2.01	21.26	0.466	0.197	41.35	
GROTH	32462	215.1704	53.1138	20.8	2	1.61	21.49	0.442	0.202	41.28	0.2004(6)
GROTH	36896	214.9730	53.3764	29.4	1	3.29	21.14	0.373	0.199	41.57	
GROTH	7430	214.4311	52.4683	104.6	1	7.67	21.80	-0.101	0.211	42.00	0.2092(7)
GROTH	5087	214.5594	52.3956	44.6	3	1.23	22.61	0.746	0.215	41.22	
GROTH	34512	214.2955	53.1980	70.2	1	5.44	21.29	2.580	0.215	41.87	0.2139(6)
GROTH	8885	215.6107	52.5075	42.4	2	2.45	21.94	0.379	0.221	41.55	
GROTH	2368	214.5933	52.3067	54.2	2	1.89	22.35	0.655	0.242	41.52	
GROTH	18322	214.5216	52.7522	25.8	2	2.78	21.63	0.335	0.247	41.71	0.24438(8)
GROTH	2682	214.7013	52.2986	19.3	3	1.52	22.03	0.370	0.244	41.44	
GROTH	5715	214.2262	52.4111	27.7	1	3.59	21.51	0.507	0.250	41.83	0.24678(8)
GROTH	19002	214.4387	52.7719	59.9	1	2.94	22.09	0.265	0.248	41.74	0.24419(8)
GROTH	17005	215.1805	52.7188	26.0	2	2.87	21.59	0.304	0.252	41.74	
GROTH	4719	214.8114	52.3908	25.3	3	1.42	22.16	0.394	0.257	41.46	

Table 2—Continued

Field (1)	ID (2)	RA (3)	DEC (4)	EW (5)	Q (6)	Ly α Flux (7)	FUV (8)	COLOR (9)	z (10)	L(Ly α) (11)	z0 (12)
GROTH	20285	215.1330	52.7994	30.9	1	4.11	21.13	0.401	0.256	41.92	
GROTH	21404	215.1861	52.8351	25.3	1	2.53	21.64	0.290	0.256	41.70	
GROTH	12279	214.3008	52.5991	19.6	2	2.08	21.76	0.527	0.264	41.65	0.26113(8)
GROTH	14069	215.3526	52.6555	29.0	2	1.80	22.28	0.463	0.260	41.57	
GROTH	21024	214.7318	52.8245	41.0	2	2.01	21.13	-0.026	0.269	41.65	0.2633(6)
GROTH	36336	214.5818	53.3393	40.3	3	2.24	22.29	1.265	0.268	41.70	
GROTH	37457	214.7951	53.2660	90.7	1	4.38	21.90	0.925	0.266	41.98	
GROTH	3488	214.9704	52.3502	40.4	2	2.52	21.83	0.541	0.269	41.75	
GROTH	37380	215.1904	53.3248	26.1	2	1.93	21.70	0.472	0.269	41.64	
GROTH	3525	214.7796	52.3522	55.2	2	2.41	22.15	0.766	0.271	41.74	
GROTH	29573	214.8762	53.0349	23.9	3	1.32	22.05	0.586	0.271	41.48	
GROTH	31403	214.2910	53.0867	33.5	1	2.25	21.86	0.570	0.270	41.71	
GROTH	33559	214.9025	53.1601	23.0	2	1.77	22.02	0.377	0.273	41.61	
GROTH	17867	215.8429	52.7425	22.0	3	1.21	22.36	0.621	0.282	41.48	
GROTH	17525	215.8241	52.7135	31.9	3	2.62	21.77	0.756	0.283	41.82	
GROTH	9045	214.9070	52.5070	24.5	2	1.86	21.75	0.475	0.286	41.68	
GROTH	15686	215.9047	52.6719	26.6	2	2.21	21.73	0.461	0.287	41.76	
GROTH	13305	215.8867	52.6237	24.6	3	1.70	21.96	0.471	0.286	41.64	
GROTH	21579	214.2081	52.8388	31.1	2	1.71	21.99	0.501	0.287	41.65	
GROTH	28751	214.7328	52.9926	42.5	1	2.92	21.88	0.509	0.290	41.89	
GROTH	23096	215.5339	52.8738	70.4	1	3.80	22.52	1.220	0.307	42.06	
GROTH	29558	214.0695	53.0259	65.7	2	2.58	22.18	1.077	0.329	41.96	
GROTH	19364	215.7761	52.7797	45.3	1	2.67	22.01	0.681	0.347	42.04	
GROTH	5549	215.4769	52.4065	28.3	2	4.24	21.22	0.832	0.350	42.24	
GROTH	10182	214.3223	52.5384	55.7	3	4.89	21.85	0.354	0.461	42.59	
NGPDWS	28760	219.1979	35.4351	115.0	1	20.66	20.93	0.061	0.180	42.27	
NGPDWS	23216	218.6954	35.2844	34.0	1	4.09	21.42	0.543	0.192	41.63	
NGPDWS	32840	219.2433	35.5977	20.9	2	2.32	21.46	0.771	0.209	41.47	
NGPDWS	11927	219.1004	34.9935	48.9	1	4.34	21.57	0.267	0.216	41.77	
NGPDWS	19918	219.1990	35.1757	26.2	3	3.74	21.13	0.711	0.253	41.86	
NGPDWS	23690	219.8446	35.3075	41.2	1	5.88	21.12	0.150	0.250	42.05	
NGPDWS	28521	219.0262	35.4586	23.9	1	4.05	21.57	0.189	0.253	41.90	
NGPDWS	35813	219.0558	35.7291	30.4	2	3.70	21.47	0.084	0.263	41.90	
NGPDWS	33782	219.5770	35.6305	78.2	1	6.05	21.63	0.521	0.264	42.11	
NGPDWS	10002	219.0922	34.9421	30.8	1	4.33	21.47	0.312	0.272	42.00	
NGPDWS	6731	219.1529	34.8428	51.7	1	10.10	21.15	0.496	0.283	42.41	
NGPDWS	2111	219.3562	34.6855	35.3	1	3.67	21.64	0.641	0.292	42.00	
NGPDWS	30997	218.7306	35.5246	19.4	2	3.13	21.11	0.523	0.320	42.02	
NGPDWS	1133	219.1333	34.6415	153.0	3	4.86	22.46	1.074	0.358	42.33	
NGPDWS	27558	219.1931	35.4176	117.0	3	6.02	22.20	0.993	0.372	42.46	
NGPDWS	10713	219.7463	34.9603	69.3	3	5.16	21.94	0.647	0.374	42.40	
NGPDWS	6321	219.7806	34.8359	77.2	3	7.43	22.32	0.944	0.374	42.55	
NGPDWS	35880	219.2820	35.6919	161.0	3	4.69	22.79	1.859	0.468	42.58	
NGPDWS	4226	219.3340	34.7577	56.0	1	6.49	21.53	0.350	0.328	42.36	
SIRTFLL	14450	259.2110	59.9642	41.8	1	22.19	19.77	0.133	0.185	42.33	

Table 2—Continued

Field (1)	ID (2)	RA (3)	DEC (4)	EW (5)	Q (6)	Ly α Flux (7)	FUV (8)	COLOR (9)	z (10)	L(Ly α) (11)	z0 (12)
SIRTFFL	14297	258.6840	59.9474	28.4	2	2.52	21.62	0.494	0.219	41.55	
SIRTFFL	14085	258.1492	59.9468	15.8	2	2.87	20.99	0.624	0.225	41.63	
SIRTFFL	10895	258.5918	59.8333	49.5	1	6.18	21.28	0.192	0.233	42.00	
SIRTFFL	958	258.8205	59.3897	30.2	2	3.45	21.03	0.547	0.235	41.76	
SIRTFFL	4246	259.8606	59.5599	49.9	2	3.58	21.57	0.556	0.237	41.78	
SIRTFFL	2856	259.3800	59.4875	33.6	2	4.72	20.94	0.610	0.302	42.14	

Note. — Col.(5): Ly α equivalent width (\AA). Col.(6): Quality of the detection (1 good; 2 fair; 3 uncertain). Col.(7): Emission line flux in $10^{-15} \text{ erg cm}^{-2} \text{ s}^{-1}$. Col.(8): FUV magnitude (in the AB system) from *GALEX* photometry. Col.(9): FUV-NUV color from *GALEX* photometry. Col.(10): Redshift assuming that the emission feature is Ly α . Col.(11): Ly α luminosity in $\log(\text{erg s}^{-1})$. Col.(12): Redshift found in the literature (NED) and references: (1) 2dF (<http://www.mso.anu.edu.au/2dFGRS/>), (2) COMBO-17 Wolf et al. (2004), (3) Vanzella et al. (2006), (4) SRS Way et al. (2005), (5) LCRS Sheth et al. (1996), (6) SDSS, (7) DEEP1 Groth Strip Weiner et al. (2006), (8) DEEP2 Data Release 3 Davis et al. (2007)